magnetochemistry

MDPI

Article

Binuclear Nickel Complexes of a New Di(hydroxyphenyl)imidazolate

Igor A. Nikovskiy [1,2], Kseniia M. Karnaukh [3], Dmitry Yu. Aleshin [1], Kirill A. Spiridonov [1,4], Anastasia A. Danshina [1,5], Yulia V. Nelyubina [1,2], Alexander V. Polezhaev [1,2] and Valentin V. Novikov [1,5,*]

1 Nesmeyanov Institute of Organoelement Compounds, Russian Academy of Sciences, Vavilova Str. 28, 119991 Moscow, Russia
2 BMSTU Center of National Technological Initiative "Digital Material Science: New Material and Substances", Bauman Moscow State Technical University, 2nd Baumanskaya Str. 5, 105005 Moscow, Russia
3 Department of Chemistry and Biochemistry, University of California, Santa Barbara, CA 93106, USA
4 Department of Chemistry, Lomonosov Moscow State University, Leninskiye Gory, 1-3, 119991 Moscow, Russia
5 Moscow Institute of Physics and Technology, National Research University, Institutskiy per. 9, Dolgoprudny, 141700 Moscow Region, Russia
* Correspondence: novikov84@ineos.ac.ru; Tel.: +7-499-135-6363

Abstract: Here, we report a new di(hydroxyphenyl)imidazolate ligand with an N_2O_2 donor set synthesized by a modified Debus–Radziszewski procedure. Its binuclear nickel(II) complexes feature a weak antiferromagnetic interaction with $J_{12} = -3.16$ cm^{-1} between the two nickel(II) ions identified by magnetometry measurements. As follows from cyclic voltammetry experiments and DFT calculations, they undergo ligand-centered oxidation via the formation of cation radicals with short lifetimes that can be potentially stabilized by bulkier t-butyl groups in the *ortho*-positions of the ligand. The reported ligand widens the range of the building blocks available to molecular magnetism community and thus provides new ways to the design of magnetic materials with switchable properties.

Keywords: mixed-valence complexes; nickel(II) complexes; binuclear complexes; antiferromagnetic interaction

Citation: Nikovskiy, I.A.; Karnaukh, K.M.; Aleshin, D.Y.; Spiridonov, K.A.; Danshina, A.A.; Nelyubina, Y.V.; Polezhaev, A.V.; Novikov, V.V. Binuclear Nickel Complexes of a New Di(hydroxyphenyl)imidazolate. *Magnetochemistry* **2022**, *8*, 132. https://doi.org/10.3390/magnetochemistry8100132

Academic Editor: Salah Massoud

Received: 20 September 2022
Accepted: 14 October 2022
Published: 18 October 2022

1. Introduction

Switchable molecular compounds that experience an intramolecular electron transfer if triggered by an external stimulus (temperature, pressure or light irradiation) are sought for their potential use in spintronics, sensorics and multifunctional devices [1,2]. This ability is common in mixed-valence systems [3,4] that contain at least two redox sites in different oxidation states and a bridging ligand to mediate metal–metal interactions. A redox active ligand, e.g., dioxolene [5,6], is often chosen as a second active site to promote metal–ligand electron-transfer. One-electron oxidation of some dioxolene complexes results in temperature- [7] or ligand geometry-dependent [8] products that feature valence tautomerism between a high-valent metal–dioxolene and a metal-semiquinone radical state [3,7,9]. While most mononuclear dioxolene complexes have only one characteristic oxidation state [9], salen-type complexes with N_2O_2 donor–ligands are prone to valence tautomerism [10,11]. Examples of di- or trinucleating phenolate-containing ligands are rare [12].

Metal complexes of stable phenoxyl radicals are targeted as catalysts that mimic galactose oxidase and glyoxal oxidase [13,14], a feature that boosted the interest in coordination compounds of phenoxyl radicals. Mixed-valence polymetallic complexes containing such radicals may be of use in information storage and integrated molecular-sized devices owing to their ability to reversibly change the electronic structure of a molecule [9].

Much of the recent efforts have been invested into understanding the influence of the bridging moiety on the rate of the electron transfer process [15]. Nitrogen-containing heterocyclic ligands are known to facilitate magnetic interactions between the metal ions through

their π-system [15], as in ruthenium complexes of doubly chelating bridging ligands, 2,2 -bipyrimidine [16], 2,2-azobis(pyridine) [17], 1,2,5-oxadiazole [18] and imidazole [19].

Here, we synthesized a new di(hydroxyphenyl)imidazolate ligand with a N_2O_2 donor set, **L**, which contains an extended π-conjugated system and a bridging imidazole moiety (Scheme 1). A comprehensive study of its two binuclear nickel complexes **[(bipy)$_4$Ni$_2$(L)]Cl** and **[(phen)$_4$Ni$_2$(L)]Cl** by dc-magnetometry, electrochemistry and DFT calculations showed them to feature a weak antiferromagnetic interaction between the two metal ions and to easily undergo two-step oxidation with an intermediate formation of a phenoxyl radical.

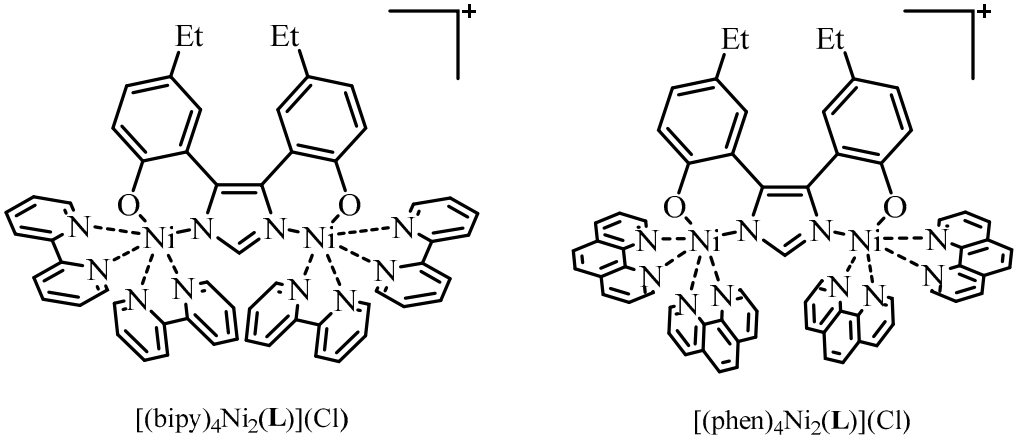

Scheme 1. Complexes in this study.

2. Results and Discussion

2.1. Synthesis

The target ligand **L** was obtained in a high yield by a four-step synthetic procedure. The first step is the acylation of 4-ethylphenol by oxalyl chloride in the presence of aluminum chloride (Scheme 2, see Figure S1 for NMR spectra). Attempts to create an imidazole moiety directly from the obtained diketone were unsuccessful due to a side condensation of phenol moiety and formaldehyde [20]. To avoid the latter from occurring, protecting methyl groups were introduced into the diketone by reacting it with dimethyl sulphate (Figure S2). A subsequent reaction with urotropine as a source of formaldehyde and ammonia acetate in a closed vessel at the boiling point of the solvent (acetic acid) produced methylated 4,5-di(2-hydroxyphenyl)imidazolate with the conversion of ca. 80% and no traces of side products (Figure S3). Note that a multicomponent Debus–Radziszewski reaction rarely proceeds with such a good conversion and a high yield [19,21]. When performing the reaction under reflux or in a closed vessel under the microwave radiation, the conversion becomes below 30%, and many by-products appear in the reaction mixture. A possible reason behind it is that the conditions of the conventional reflux method are too mild to give a high yield, and the microwave radiation causes a product to decompose.

To produce the ligand **L**, the protective methyl groups were removed by reacting methylated 4,5-di(2-hydroxyphenyl)imidazolate with boron tribromide. The formation of the target product was confirmed by NMR spectroscopy; its ^{1}H NMR spectrum feature a singlet at 7.68 ppm, which is characteristic of the CH proton of the imidazole moiety (Figure S4), and no signals of the methoxy groups, which confirms the deprotection.

Binuclear Ni^{2+} complexes **[(bipy)$_4$Ni$_2$(L)]Cl** and **[(phen)$_4$Ni$_2$(L)]Cl** (Scheme 1) were synthesized by the template reaction of the obtained ligand **L** and complexes bipy$_2$NiCl$_2$ and phen$_2$NiCl$_2$, respectively, in the presence of DBU as a noncoordinating base in methanol. Attempts to use trimethylamine for this purpose failed due to the formation of trimethylamine metal complexes [22]. The successful formation of the target Ni^{2+} complexes was confirmed by elemental analysis, NMR spectroscopy (although a full assignment of signals in the ^{1}H NMR spectrum was complicated by the paramagnetic nature of the complexes;

Figures S5 and S6) and X-ray diffraction. **[(bipy)$_4$Ni$_2$(L)]Cl** is soluble in methanol and DMF; **[(phen)$_4$Ni$_2$(L)]Cl** is slightly soluble only in CH_3OH.

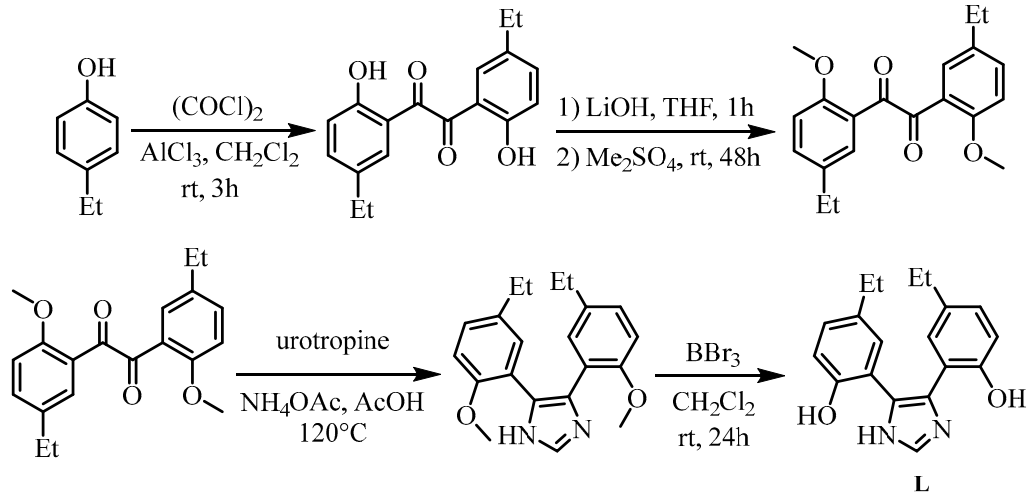

Scheme 2. Synthetic pathway to the ligand **L**.

The choice of other metal salts as a source of metal ion M (M = Fe^{3+}, Cu^{2+} or Mn^{2+}) produced, in the same reaction conditions, the unwanted homoleptic complex $[(bipy)_3M]^{n+}$ as the main product, which apparently resulted from the intramolecular disproportionation reaction occurring in the binuclear complexes. Using a Co^{2+} salt produced inseparable mixtures of dia- and paramagnetic complexes of an unknown composition.

2.2. X-ray Crystallography

The formation of the target complexes **[(bipy)$_4$Ni$_2$(L)]Cl** and **[(phen)$_4$Ni$_2$(L)]Cl** was confirmed by X-ray diffraction analysis (Figure 1) of their solvates **[(bipy)$_4$Ni$_2$(L)]Cl•2CH$_3$OH•0.75Et$_2$O** and **[(phen)$_4$Ni$_2$(L)]Cl•3CH$_3$OH** obtained by recrystallization from methanol and diethyl ether (1/1). They crystallize in the triclinic space group P-1, thereby adopting a rac form (no meso form was isolated upon fractional crystallization [19]).

In the two complexes, the imidazole moiety and both the hydroxyl groups of the ligand **L** are deprotonated; the corresponding C-O bond lengths (C-O 1.330(6)–1.340(6) Å) fall between the values typical for the double and single C–O bond (1.24 and 1.38–1.42 Å) [23]. Each of the two Ni^{2+} ions coordinates four nitrogen atoms from the two bipyridine or phenanthroline ligands (Ni–N 2.061(5)–2.146(6) Å) and two heteroatoms of the ligand **L**, the nitrogen atom of its imidazole moiety and the oxygen atom of the C-O group (Ni–N 2.033(5)–2.050(4) Å, Ni–O 2.014(4)–2.050(4) Å), to produce a nearly perfect octahedral environment, as gauged by shape measures [24] (Table 1). These measures quantify how far the shape of the coordination polyhedron is from an ideal shape, such as an ideal octahedron (OC-6). For **[(bipy)$_4$Ni$_2$(L)]Cl** and **[(phen)$_4$Ni$_2$(L)]Cl**, the octahedral shape measure S(OC-6) estimated from the X-ray diffraction data for these complexes [24] is as low as 0.733 and 0.658, respectively. For comparison, the shape measure of the NiN_4O_2 coordination polyhedron respective to another ideal shape with six vertices, the trigonal prism (TR-6), adopts much higher values of 12.366–15.215.

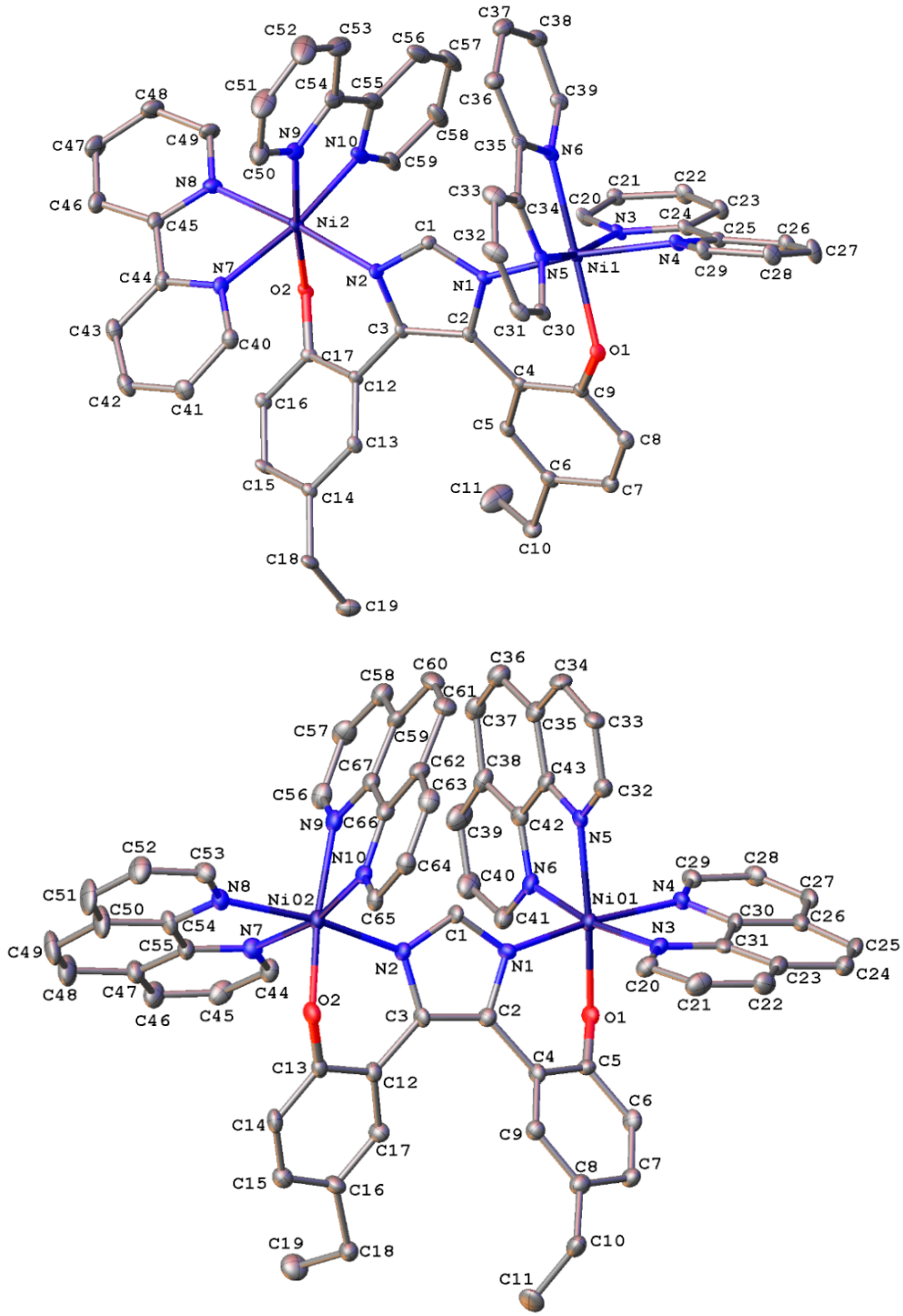

Figure 1. General view of the complex cations **[(bipy)$_4$Ni$_2$(L)]$^+$** (**top**) and **[(phen)$_4$Ni$_2$(L)]$^+$** (**bottom**) in representation of atoms via thermal ellipsoids at 20% probability level. Hydrogen atoms and minor components of the disordered ethyl groups in **[(phen)$_4$Ni$_2$(L)]Cl** are omitted.

In the crystal of the solvated complex **[(bipy)$_4$Ni$_2$(L)]Cl**, both the C-O bonds of the ligand **L** form hydrogen bonds with the lattice methanol (O ... O 2.621(6) and 2.569(5) Å, OHO 162.5(4) and 171.4(3)°). In the case of **[(phen)$_4$Ni$_2$(L)]Cl**, only one of them is involved in such a bond (O ... O 2.695(7) Å, OHO 162.7(3)°); the two other solvent molecules of methanol are hydrogen-bonded to the first methanol molecule (O ... O 2.721(7) Å,

OHO 161.3(4)°) and to the chloride anion (O ... Cl 3.065(7) Å, OHCl 175.5(3)°). In **[(bipy)$_4$Ni$_2$(L)]Cl**, the chloride anion forms only weak C-H ... Cl contacts.

Table 1. Main geometrical parameters * of **[(bipy)$_4$Ni$_2$(L)]Cl●CH$_3$OH●0.75Et$_2$O** and **[(phen)$_4$Ni$_2$(L)]Cl ●3CH$_3$OH**.

Parameters	[(bipy)$_4$Ni$_2$(L)]Cl●2CH$_3$OH●0.75Et$_2$O		[(phen)$_4$Ni$_2$(L)]Cl●3CH$_3$OH	
	Ni(1)	Ni(2)	Ni(1)	Ni(2)
Ni–N$_{Py}$, Å	2.074(5)–2.132(2)	2.061(5)–2.095(5)	-	-
Ni–N$_{Phen}$, Å	-	-	2.076(5)–2.146(6)	2.080(5)–2.135(6)
Ni–N$_L$, Å	2.040(4)	2.050(4)	2.036(6)	2.033(5)
Ni–O$_L$, Å	2.014(4)	2.050(4)	2.028(4)	2.036(5)
S(TP-6)	12.997	15.215	13.850	12.366
S(OC-6)	0.958	0.733	0.658	0.885

* The N_{Py} (N_{Phen}), N_L and O_L are the nitrogen atoms of bipyridine (phenanthroline) ligands and the nitrogen and oxygen atoms of the ligand **L**, respectively. S(TP-6) and S(OC-6) are trigonal-prismatic and octahedral shape measures, respectively.

2.3. Magnetic Susceptibility Measurements

To probe if the extended π-conjugated system of the ligand **L** mediates magnetic interactions between the two Ni^{2+} ions in the obtained complexes, magnetic properties of a finely ground powder of desolvated **[(bipy)$_4$Ni$_2$(L)]Cl** were accessed in the solid state by the dc-magnetometry (Figure 2, left); a solid sample of **[(phen)$_4$Ni$_2$(L)]Cl** suffered amorphization upon grinding to avoid magnetic torquing under the applied magnetic field [25] and therefore was not probed by this method. For **[(bipy)$_4$Ni$_2$(L)]Cl**, the behavior of the magnetic susceptibility in the temperature range of 2–300 K is consistent with a weak antiferromagnetic interaction between the two Ni^{2+} ions. At the highest accessible temperature of 300 K, the χ_mT product adopts the value of 2.21 cm^{3}K/mol, which is close to the spin-only value (2.0 cm^{3}K/mol) for two independent Ni^{2+} ions with no significant zero-field splitting or exchange effects. Upon cooling to 100 K, the magnetic susceptibility gradually decreases to a nearly constant value of 2.2 cm^{3}K/mol. The drop below 100 K is a sign of antiferromagnetic exchange interactions between the two Ni^{2+} ions (Figure 2, left). The best fit of the resulting temperature-dependence of the χ_mT product with the isotropic g_{iso} value of the g-tensor [26] to avoid overparameterization was obtained with g_{iso} of 2.09 and the exchange constant J_{12} of -3.16 cm^{-1}; a weak antiferromagnetic interaction with J_{12} of -2.15 to -1.43 cm^{-1} also follows from DFT calculations (see below).

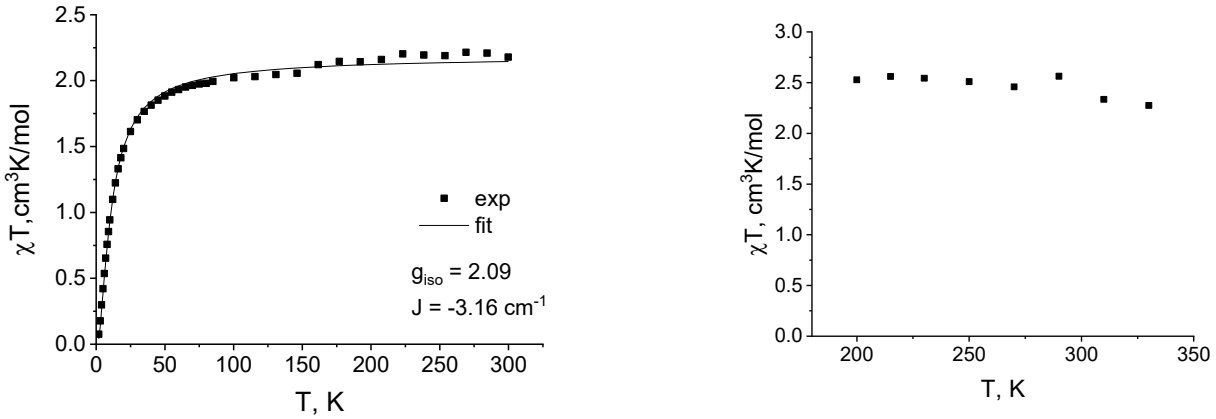

Figure 2. Variable-temperature magnetic susceptibility for a microcrystalline sample (**left**) and a methanol solution (**right**) of **[(bipy)$_4$Ni$_2$(L)]Cl** from the dc-magnetometry and the Evans technique, respectively. For the magnetic susceptibility of a methanol solution of **[(phen)$_4$Ni$_2$(L)]Cl**, see Figure S7.

The magnetic susceptibility for both the complexes, **[(bipy)$_4$Ni$_2$(L)]Cl** and **[(phen)$_4$Ni$_2$(L)]Cl**, was also measured in their methanol solutions (Figure 2, right) by the Evans technique [27] of the NMR spectroscopy often used for this purpose [28]. For **[(bipy)$_4$Ni$_2$(L)]Cl**, the χ_mT product is constant at ca. 2.5 cm^{3}K/mol over the entire temperature range of 200–330 K accessible in methanol. The observed value is higher than the spin-only value for two independent Ni^{2+} ions; however, with a claimed accuracy of the Evans technique of ~11% [29], it is consistent with dc-magnetometry data.

2.4. Redox Properties

To check for the possible formation of mixed-valence species, redox properties of the ligand L and its complexes **[(bipy)$_4$Ni$_2$(L)]Cl** and **[(phen)$_4$Ni$_2$(L)]Cl** were probed by cyclic voltammetry (Figure 3). In the corresponding measurements, two cycles were used to highlight the stability of possible intermediates. For **L**, an irreversible one-electron oxidation wave with the highest oxidation potential at Ep = 0.378 V vs. Fc/Fc$^+$ indicates a low stability of the phenoxyl radical produced upon the ligand oxidation [30]. The cyclic voltammograms of the Ni^{2+} complexes feature two reversible oxidation waves at $E^1_{1/2}$ = −0.194 V and $E^2_{1/2}$ = 0.120 V for **[(bipy)$_4$Ni$_2$(L)]Cl**, hinting on the formation of two phenoxyl radicals on both sides of a binuclear complex (Scheme 3), as gauged by higher potentials of the redox couple Ni^{2+}/Ni^{3+} [31]. An increase in the degree of reversibility of the oxidation process as compared to the parent ligand **L** is a sign of the stabilization of the phenoxyl radicals and of a substantial contribution of the orbitals of the metal ions to the overall stability of the complex, which increases the lifetime of the radical [30]. It is, however, a common wisdom that bulky groups (especially those located in *ortho*- and *para*-positions of the phenol moiety [12,30]) stabilize the radicals, as is, probably, the case of the complex **[(bipy)$_4$Ni$_2$(L)]Cl** with bulky *para*-ethyl groups in the ligand **L** and the bipy ligands.

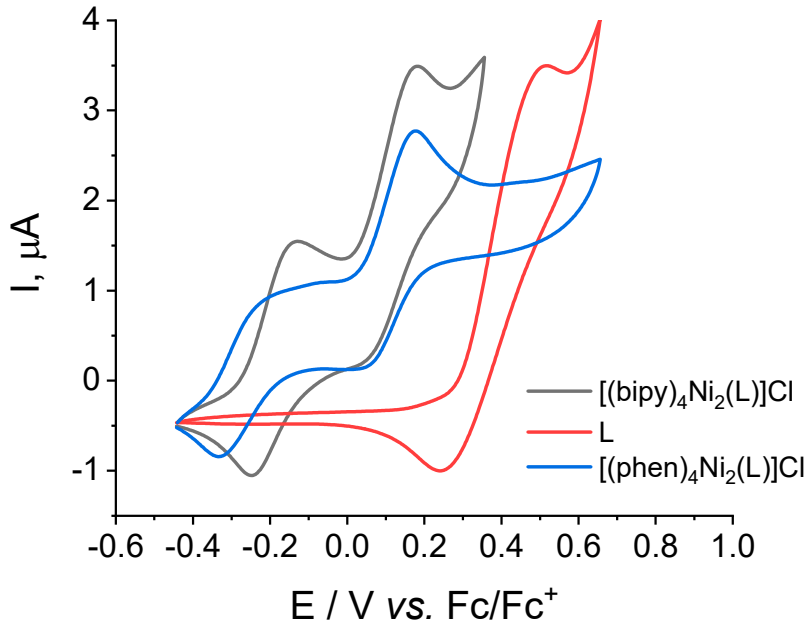

Figure 3. Cyclic voltammograms of the ligand **L** (red line) and of the complexes **[(bipy)$_4$Ni$_2$(L)]Cl** (black line) and **[(phen)$_4$Ni$_2$(L)]Cl** (blue line) in 0.1 M $TBAPF_6/CH_3OH$ solutions at a scan rate of 0.10 V s^{-1}. All potentials are referenced to ferrocene/ferrocenium (Fc/Fc$^+$) as an internal reference redox couple.

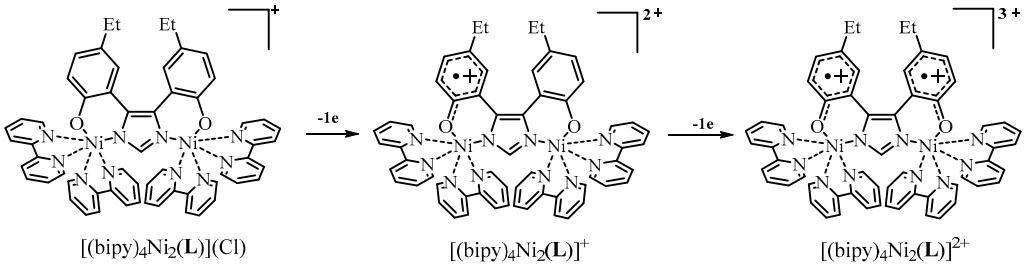

Scheme 3. A scheme of the stepwise oxidation of the ligand.

The same stabilization occurs for **[(phen)$_4$Ni$_2$(L)]Cl**, as two reversible oxidation waves are observed at even lower values of $E^1_{1/2} = -0.270$ V and $E^2_{1/2} = 0.116$ V. Unfortunately, all our attempts to chemically oxidize the complexes **[(bipy)$_4$Ni$_2$(L)]Cl** and **[(phen)$_4$Ni$_2$(L)]Cl** with $Ag(BF_4)$, Br_2 or $Fc[PF_6]$ resulted in mixtures of paramagnetic products, the major of them being the initial complex $(bipy)_2NiCl_2$ as identified by NMR spectroscopy. This failure can be explained by the formation of a ligand radical with a short lifetime due to the absence of t-butyl groups in its *ortho*-positions, the common stabilizing substituents that protect phenoxy radicals from bis(μ-phenolate) dimerization [32].

2.5. DFT Calculations

To confirm the ligand-centered nature of the oxidation of the complexes **[(bipy)$_4$Ni$_2$(L)]Cl** and **[(phen)$_4$Ni$_2$(L)]Cl** that proceeds via the formation of unstable cation radicals, DFT calculations with the popular hybrid functional B3LYP [33] were performed for the complex cation **[(bipy)$_4$Ni$_2$(L)]$^+$** and the product of its oxidation, **[(bipy)$_4$Ni$_2$(L)]$^{2+}$**. The chosen functional is the best for describing one-electron-oxidized nickel(II) complexes with the phenol-containing ligands, such as a salen-type complex featuring di-t-butyl groups in its ligand [34].

The frontier computed MOs of the cation **[(bipy)$_4$Ni$_2$(L)]$^+$** are of a π-character; α-HOMO and β-HOMO (Figure 4) are localized on the imidazole and ethylphenol moieties and the oxygen atoms of the phenolate moieties of the ligand **L** with only a small contribution from the d-orbitals of the Ni^{2+} ions, thereby supporting the above conclusion on the ligand-centered nature of the oxidation of the complexes **[(bipy)$_4$Ni$_2$(L)]Cl** and **[(phen)$_4$Ni$_2$(L)]Cl**. In contrast, α-LUMO and β-LUMO are localized on the bipyridine ligands (Figure S8). The spin density is distributed over two metal Ni^{2+} ions, residing on the nitrogen and oxygen atoms of the ligands and both the metal ions (Figure 4). The exchange constant J_{12} calculated with the broken symmetry approach, which allows extracting a phenomenological constant in Heisenberg–Dirac–van Vleck Hamiltonian [35–37], is in the range of -2.15 to -1.43 cm^{-1}.

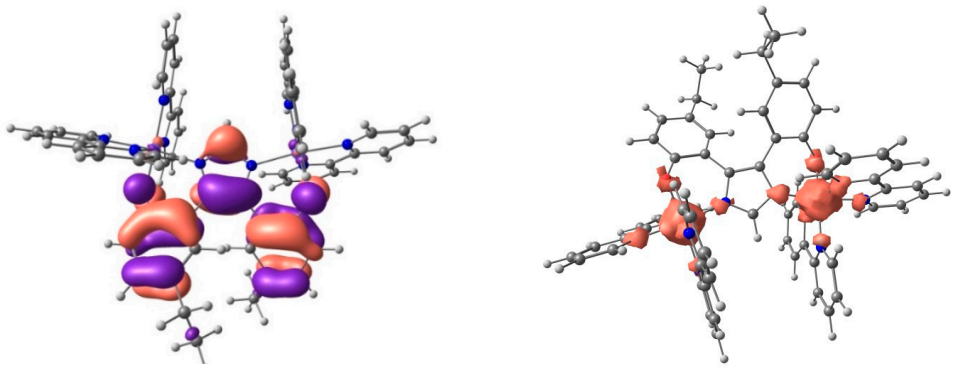

Figure 4. General view of (**a**) α-HOMO (0.03 isosurface level; EHOMO = −0.1656 a.u.) and (**b**) spin density (0.0065 isosurface level) in the cation **[(bipy)$_4$Ni$_2$(L)]$^+$**.

The calculated energy level diagrams for **[(bipy)$_4$Ni$_2$(L)]$^+$** and **[(bipy)$_4$Ni$_2$(L)]$^{2+}$** (Figure 5) show that β-MOs in the nonoxidized species lie lower than α-MOs. The same pattern is observed for the oxidized species. In this case, however, the energy difference between α- and β-MOs is larger, e.g., $|\Delta E|$ for α-273 and β-268 is 0.0096 a.u. The MOs of **[(bipy)$_4$Ni$_2$(L)]$^{2+}$** are lower in energy than those in **[(bipy)$_4$Ni$_2$(L)]$^+$**, with $|\Delta E^{HOMO}|$ equal to 0.032 a.u.

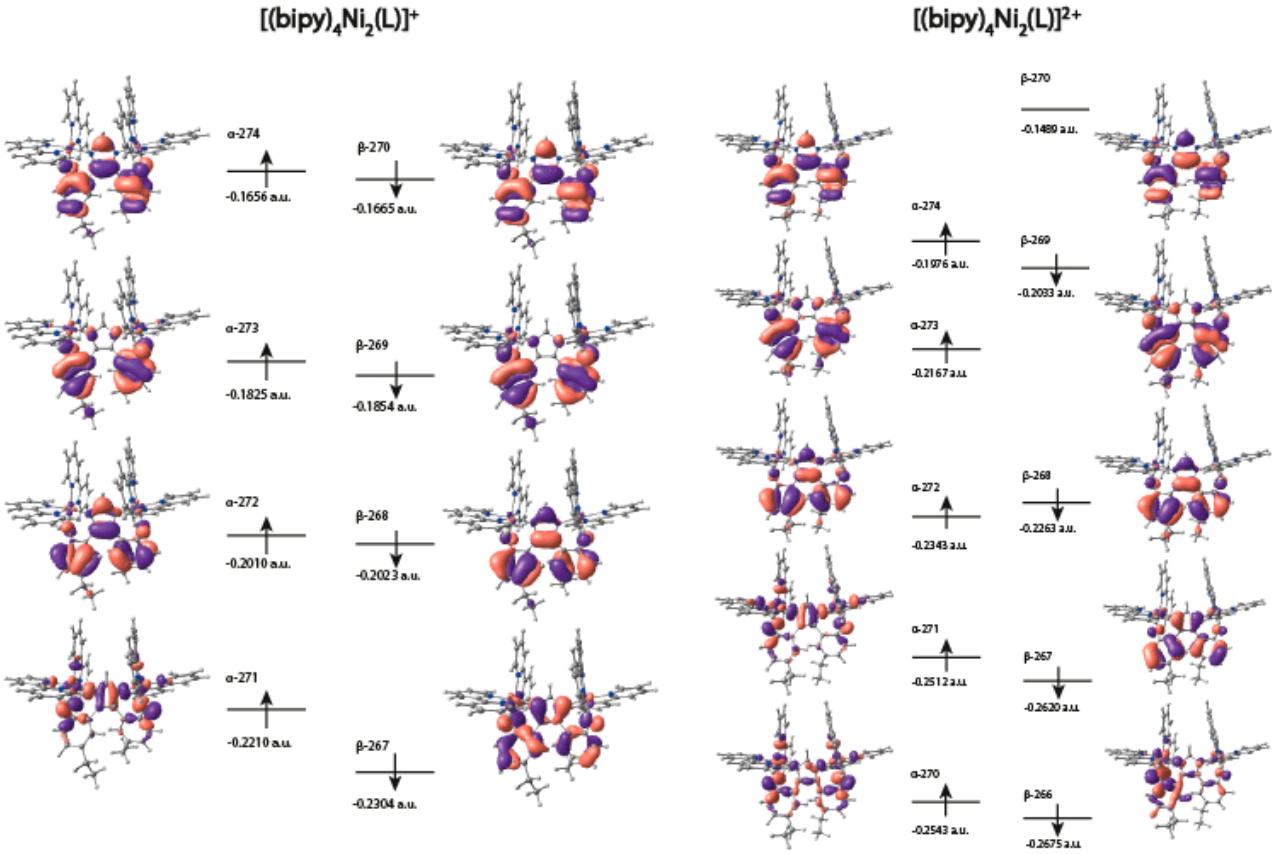

Figure 5. Calculated energy level diagram for α- and β-MOs in the cation **[(bipy)$_4$Ni$_2$(L)]$^+$** and its oxidized form **[(bipy)$_4$Ni$_2$(L)]$^{2+}$**.

For the oxidized species **[(bipy)$_4$Ni$_2$(L)]$^{2+}$**, the frontier α-orbitals are very similar to those in the complex cation **[(bipy)$_4$Ni$_2$(L)]$^+$** (Figures 4, 6, S8 and S9); however, the spin density distribution is quite different (Figure 5). In **[(bipy)$_4$Ni$_2$(L)]$^{2+}$**, it has an out-of-plane π-character and is located on the carbon atoms of the phenyl rings, the oxygen atoms of the phenolate moieties of the ligand **L** and the nitrogen atoms of the bipy ligands (Figure 6). Some of the spin density is also located on the two nickel ions. The same trend is observed for **[(phen)$_4$Ni$_2$(L)]$^{2+}$** (see Figures S10–S12). These results confirms that upon one-electron oxidation, the electron leaves the ligand site rather than a Ni^{2+} ion, thereby explaining a short lifetime of the oxidized species and the difficulties that we experienced while attempting to chemically oxidize the complexes **[(bipy)$_4$Ni$_2$(L)]Cl** and **[(phen)$_4$Ni$_2$(L)]Cl**.

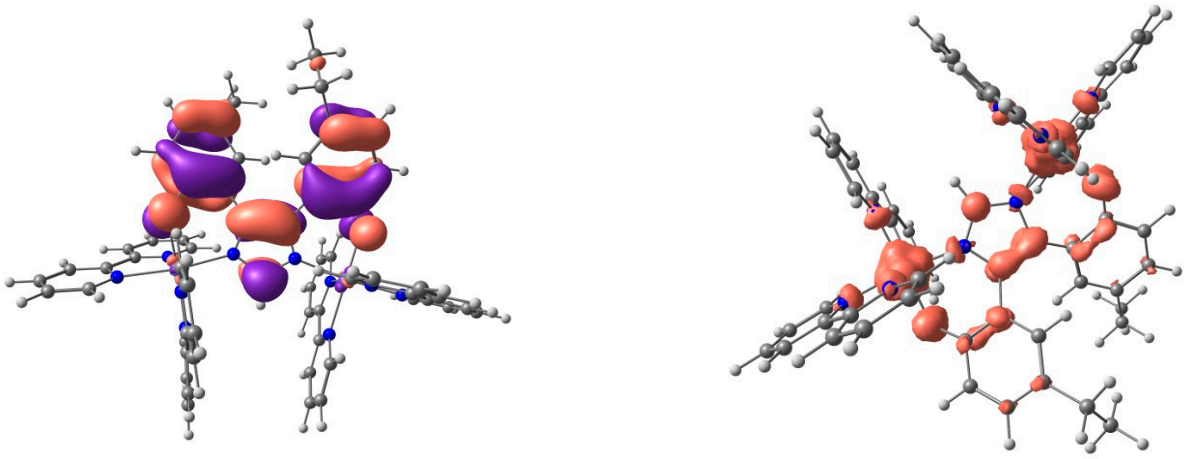

(**a**) (**b**)

Figure 6. General view of (**a**) α-HOMO (0.03 isosurface level; EHOMO = −0.1976 a.u.) and (**b**) spin density (0.0065 isosurface level) in the cation **$[(bipy)_4Ni_2(L)]^{2+}$**.

3. Materials and Methods

Synthesis. All synthetic manipulations were carried out on air unless stated otherwise. Solvents were purchased from commercial sources and purified by distilling from conventional drying agents under an argon atmosphere prior to use. 2,2′-Bipyridine and 1,10-phenanthroline were obtained from Aldrich, and $(bipy)_2NiCl_2$ and $(phen)_2NiCl_2$ were synthesized by the reported procedure [38].

1,2-bis(5-ethyl-2-hydroxyphenyl)ethane-1,2-dione. 4-Ethylphenol (25.65 g, 0.21 mol) was dissolved in 50 mL of methylene chloride, and the solution was added dropwise to a suspension of aluminum chloride (56 g, 0,42 mol) in 300 mL of dichloromethane. The resulting mixture was stirred for 30 min. At some point, a solution of oxalyl chloride (8.6 mL, 0.1 mol) in 50 mL of dichloromethane was added dropwise to produce a dark-colored solution that was then stirred at r.t. for 10 h. A 12 M HCl solution was carefully added while cooling with an ice bath to quench the reaction mixture and thereby avoid its overheating. The resulting suspension was filtered, and the filtrate was washed with dichloromethane. The mother liquor that contained both the organic and aqueous phases was extracted with dichloromethane, dried over magnesium sulfate ($MgSO_4$), filtered and evaporated. The dry residue was recrystallized from ethanol at −10 °C. Yield: 59% (36.96 g). ^{1}H NMR ($CDCl_3$, 400 MHz): δ (ppm) = 11.21 (s, 2H, OH), 7.45 (dd, 2H, $^2J_{HH}$ = 8.7 Hz, Ph), 7.24 (d, 2H, $^2J_{HH}$ = 2.2 Hz, Ph), 7.04 (d, 2H, $^2J_{HH}$ = 8.6 Hz, Ph,), 2.54 (q, 2H, $^2J_{HH}$ = 7.6 Hz, $2CH_2$), 1.15 (t, 6H, $^2J_{HH}$ = 7.6 Hz, $2CH_3$,). ^{13}C NMR ($CDCl_3$, 101 MHz): δ (ppm) = 196.49, 161.84, 138.54, 135.70, 130.69, 118.69, 27.74, 15.58.

1,2-bis(5-ethyl-2-methoxyphenyl)ethane-1,2-dione. In a 250 mL round-bottom flask, a solution of 1,2-bis(5-ethyl-2-hydroxyphenyl)ethane-1,2-dione (5.97 g, 0.02 mol) in THF and aqueous lithium hydroxide $LiOH{\cdot}H_2O$ (1.84 g, 0.04 mol) was stirred at r.t. for one hour. Dimethyl sulfate (3.13 mL, 0.04 mol) was added dropwise, and the reaction mixture was kept under stirring for 24 h. The solvent was distilled off, and the solid residue was dissolved in 2 M solution of sodium hydroxide, extracted with dichloromethane, dried over magnesium sulfate and filtered off. The solvent was evaporated, and the residue was dried under high vacuum. Yield: 82% (5.35 g). ^{1}H NMR ($CDCl_3$, 400 MHz): δ (ppm) = 7.96 (d, 2H, $^2J_{HH}$ = 2.4 Hz, Ph), 7.45 (dd, 2H, $^2J_{HH}$ = 8.5 Hz, Ph), 6.94 (d, 2H, $^2J_{HH}$ = 8.5 Hz, Ph), 3.63 (s, 6H, $2CH_3$), 2.72 (c, 4H, $^2J_{HH}$ = 7.6 Hz, $2CH_2$), 1.31 (t, 6H, $^2J_{HH}$ = 7.6 Hz, $2CH_3$). Calcd for $C_{20}H_{22}O_4$ %: C 73.60%, H 6.79%. Found, %: C 73.58%, H 6.82%.

4,5-bis(5-ethyl-2-methoxyphenyl)-1H-imidazole. In a 25 mL thick-walled Schlenk flask with a Teflon screw stopper and a magnetic stirrer, 1,2-bis(5-ethyl-2-methoxyphenyl)ethane-1,2-dione (1.68 g, 0.005 mol) was added to 20 mL of acetic acid together with urotropine (1.59 g, 0.011 mol) and ammonium acetate (7.95 g, 0.1 mol). The mixture was stirred for

8 h at 120 °C and then poured into a 30% aqueous ammonia solution, extracted with ethyl acetate and dried over magnesium sulfate; the solvent was distilled off. The product was purified by flash chromatography; the starting compound was first eluted with ethyl acetate, and the final product with ethyl acetate-methanol (1:5). Yield: 72% (1.21 g). ^{1}H NMR ($CDCl_3$, 400 MHz): δ (ppm) = 7.68 (s, 1H, CH=N), 7.17 (d, 2H, $^{2}J_{HH}$ = 2.2 Hz, Ph), 7.04 (d.d, 2H, $^{2}J_{HH}$ = 8.4 Hz, Ph), 6.82 (d, 2H, $^{2}J_{HH}$ = 8.3 Hz, Ph), 3.67 (s, 6H, $2CH_3$), 2.46 (q, 4H, $^{2}J_{HH}$ = 7.6 Hz, $2CH_2$), 1.07 (t, 6H, $^{2}J_{HH}$ = 7.6 Hz, $2CH_3$). ^{13}C NMR ($CDCl_3$, 151 MHz): δ (ppm) = 154.05, 136.32, 133.68, 129.67, 127.58, 110.92, 55.51, 27.87, 15.71. Calcd for $C_{21}H_{24}N_2O_2$ %: C 74.97%, H 7.19%, N 8.33%. Found, %: C 74.91%, H 7.22%, N 8.27%.

2,2′-(1H-imidazole-4,5-diyl)bis(4-ethylphenol) (L). In a Schlenk flask (50 mL) under argon, 4,5-bis(5-ethyl-2-methoxyphenyl)-1H-imidazole (1.01 g, 0.003 mol) was dissolved in 15 mL of dry dichloromethane. The solution was cooled to −10 °C, and a solution of boron tribromide (1.13 mL, 0.012 mol) in 15 mL of dry dichloromethane was added dropwise. The resulting mixture was warmed to r.t. and stirred for 24 h at this temperature. Then, ethanol (2.7 mL) was carefully added to the mixture at −10 °C that was stirred for another 2 h. The precipitate was filtered off, washed with dichloromethane, added to a solution of Na_2CO_3, and then with distilled water. The product was dried under high vacuum. Yield: 59% (0.55 g). ^{1}H NMR (DMSO-d6, 400 MHz): δ (ppm) = 10.01 (s, 2H, OH, NH), 9.20 (s, 1H, CH=N), 7.15–7.02 (m, 2H, Ph), 6.93 (dd, 4H, $^{2}J_{HH}$ = 8.3 Hz, Ph), 2.37 (q, 4H, $^{2}J_{HH}$ = 7.6 Hz, CH_2), 0.97 (t, 6H, $^{2}J_{HH}$ = 7.5 Hz, CH_3). ^{13}C NMR (DMSO-d6, 101 MHz): δ (ppm) = 153.71, 134.49, 130.69, 129.92, 126.39, 116.26, 27.43, 16.03. Calcd for $C_{19}H_{20}N_2O_2$ %: C 74.00%, H 6.54%, N 9.08%. Found, %: C 73.96%, H 6.57%, N 9.05%.

[(bipy)$_4$Ni$_2$(L)]Cl. The ligand **L** (100 mg, 0.32 mmol) was dissolved with DBU (0.145 mL, 0.97 mmol) in 15 mL of methanol and stirred for 10 min. $(bipy)_2NiCl_2$ (322 mg, 0.68 mmol) in 10 mL of methanol was quickly added to this solution. The resulting mixture was stirred for 3 h at r.t., evaporated under reduced pressure and recrystallized from a mixture of methanol/diethyl ether (1/1). Yield: 121 mg (35%). ^{1}H NMR (CD_3OD; 300 MHz): δ (ppm) = 134.5–120.3 (br. m), 63.47–59.44 (br. m), 56.76 (br. s), 46.94 (br. s), 43.80–41.33 (br. m), 40.05 (br. s), 39.46 (br. s), 38.03 (br. s), 14.75 (br. s), 13.66–13.46 (br. m),12.46 (br. s), 11.83–10.99 (br. m), 9.63 (br. s), −2.4 (br. s), −5.2 (br. s). UV-vis in CH_3OH: λ(max) = 340 nm. Calcd for ($C_{59}H_{51}ClN_{10}Ni_2O_2$•$2CH_3OH$•$0.75C_4H_{10}O$): C 63.92%; H 5.41%; N 11.65%. Found: C 63.49%; H 5.03%; N 11.32%.

[(phen)$_4$Ni$_2$(L)]Cl. The ligand **L** (197 mg, 0.64 mmol) was dissolved with DBU (0.29 mL, 1.91 mmol) in 20 mL of methanol and stirred for 10 min. $(phen)_2NiCl_2$ (626 mg, 1.28 mmol) in 20 mL of methanol was quickly added to this solution. The resulting mixture was stirred for 3 h at r.t., and then the product was filtered off and recrystallized from methanol at –10 °C. Yield: 421 mg (55%). ^{1}H NMR (CD_3OD; 300 MHz): δ (ppm) = 133.5–122.3 (br. m), 45.82–44.04 (br. m), 42.20 (br. s), 41.22 (br. s), 23.84 (br. s), 23.06–22.26 (br. m), 21, 49 (br. s), 16.25–15.28 (br. m), 15.45 (br. s), 15.10 (br. s), 14.60 (br. s), 11.77 (br. s), 11.28 (br. s), 10.46–9.93 (br. m), −3.31 (br. m), −5.73 (br. m). UV-vis in CH_3OH: λ(max) = 366 nm. Calcd for ($C_{67}H_{51}ClN_{10}Ni_2O_2$•$3CH_3OH$): C 65.93%; H 4.82%; N 10.98%. Found: C 65.64%; H 4.62%; N 10.65%.

Analytical and Spectroscopic Measurements. ^{1}H and ^{13}C NMR spectra were recorded at 298 K with Bruker Avance 300 and 600 FT-spectrometers (300.15 and 600.22 MHz ^{1}H frequency, respectively). UV-vis spectra were recorded in methanol at room temperature with a Shimadzu UV-2600i double-beam spectrophotometer in the wavelength range from 240 to 1400 nm. The amount of carbon, nitrogen and hydrogen contained was estimated on a Carlo Erba analyzer, model 1106. Cyclic voltammograms (CV) were recorded at r.t. in the nitrogen atmosphere on an Autolab PGSTAT128N potentiostat-galvanostat in a standard three-electrode cell using a 3 mm thick glassy carbon working electrode, a platinum wire counter electrode and an Ag/AgCl reference electrode in a saturated KCl solution. The required conductivity of the solution was achieved by adding a $TBAPF_6$ to the test solution to the concentration of 0.1 M. All CV curves were measured at a potential sweep rate of 100 mV/s.

X-ray crystallography. X-ray diffraction data for the single crystals of **[(bipy)$_4$Ni$_2$(L)]Cl** and **[(phen)$_4$Ni$_2$(L)]Cl**, which were grown by slow vapor diffusion of diethyl ether into a methanol solution, were collected with Bruker APEXII DUO and Quest D8 CMOS diffractometers, using graphite monochromated Mo-Kα radiation (λ = 0.71073 Å). Using Olex2 [39], the structures were solved with the ShelXT [40] structure solution program using Intrinsic Phasing and refined with the XL [41] refinement package using least-squares minimization against F^2 in anisotropic approximation for nonhydrogen atoms. Hydrogen atoms of methanol molecules in **[(bipy)$_4$Ni$_2$(L)]Cl** and **[(phen)$_4$Ni$_2$(L)]Cl** were located via difference Fourier synthesis, while the positions of other hydrogen atoms were calculated, and they all were refined in isotropic approximation within the riding model. Crystal data and structure refinement parameters are given in Table 2. CCDC 2,207,058 and 2,207,059 contain the supplementary crystallographic data for **[(bipy)$_4$Ni$_2$(L)]Cl** and **[(phen)$_4$Ni$_2$(L)]Cl**, respectively.

Table 2. Crystal data and structure refinement parameters for **[(bipy)$_4$Ni$_2$(L)]Cl•2CH$_3$OH•0.75Et$_2$O** and **[(phen)$_4$Ni$_2$(L)]Cl•3CH$_3$OH**.

	[(bipy)$_4$Ni$_2$(L)]Cl•2CH$_3$OH•0.75Et$_2$O	**[(phen)$_4$Ni$_2$(L)]Cl•3CH$_3$OH**
Empirical formula	$C_{64}H_{64.5}ClN_{10}Ni_2O_{4.75}$	$C_{70}H_{61}ClN_{10}Ni_2O_5$
Formula weight	1202.62	1275.15
T, K	120	100
Crystal system	triclinic	triclinic
Space group	P-1	P-1
Z	2	2
a, Å	13.555(2)	12.2327(3)
b, Å	15.389(3)	13.0491(3)
c, Å	17.007(3)	20.7742(5)
α, °	77.732(3)	72.9350(10)
β, °	70.231(3)	77.2100(10)
γ, °	81.830(3)	89.9820(10)
V, Å^3	3253.0(9)	3084.00(13)
D_{calc}, (g cm^{-1})	1.228	1.373
μ, cm^{-1}	6.73	7.15
F(000)	1259	1328
$2\theta_{max}$, °	54	50
Reflections measured	45,304	41,247
Independent reflections	14,150	10,859
Observed reflections [I > 2σ(I)]	6921	5967
Parameters	756	811
R1	0.0794	0.0811
wR2	0.2188	0.2702
GOF	0.955	1.100
$\Delta\rho_{max}/\Delta\rho_{min}$ (e Å^{-3})	0.955/−0.694	2.109/−0.415

Magnetochemistry. Magnetic susceptibility of **[(bipy)$_4$Ni$_2$(L)]Cl** was measured in the temperature range 2–300 K with a Quantum Design PPMS-9 device under the dc-magnetic field of 5 kOe. A finely ground and dried microcrystalline powder (23 mg) was immobilized in mineral oil inside a polyethylene capsule. Sweep rate was 74 s/K below 100 K and 54.6 s/K above this temperature. The data were corrected for the sample holder, the mineral oil and the diamagnetic contribution, the latter by using the Pascal constants. Smoothing was performed by the Savitzky–Golay method with five points of window and polynomial order of two. To avoid overparameterization, the observed variable-temperature dc-magnetic susceptibility was fitted in PHI software [19] using the spin Hamiltonian:

$$\begin{aligned}\hat{H} = {} & \mu_\beta g_{iso}\left(B_x\hat{S}_{1x} + B_y\hat{S}_{1y} + B_z\hat{S}_{1z}\right) \\ & + \mu_\beta g_{iso}\left(B_x\hat{S}_{2x} + B_y\hat{S}_{2y} + B_z\hat{S}_{2z}\right) + J_{12}\hat{S}_1\hat{S}_2\end{aligned} \quad (1)$$

where $S = 1$ is the spin of the Ni^{2+} ion, g_{iso} is the isotropic value of the g-tensor, μ_B is the Bohr magneton and J_{12} is the exchange constant.

Evans method. The temperature dependence of the molar magnetic susceptibility (χ_M) of the complexes **[(bipy)$_4$Ni$_2$(L)]Cl** and **[(phen)$_4$Ni$_2$(L)]Cl** in methanol-d4 was evaluated in the Evans experiment. The appropriate ^{1}H NMR spectra were recorded in the temperature a range of 200–330 K using an NMR tube with a coaxial inset. The inner (control) tube contained ~1% Me_4Si in methanol-d4, and the outer tube, a solution of the complex (~1–5 mg/cm^3) in the same solvent with the same concentration of Me_4Si. The value of χ_M was calculated from the difference between the chemical shifts of Me_4Si in pure dichloromethane-d2 and in a solution of the complex ($\Delta\delta$, Hz) using the following equation:

$$\chi_M = \frac{\Delta\delta M}{\upsilon_0 S_f c} - \chi_M^{dia} \quad (2)$$

M is the molar mass of the Ni^{2+} complex, g/mol; ν_0 is the spectrometer frequency, Hz; S_f is the coefficient of the magnet shape ($4\pi/3$); c is the concentration of the complex, g/cm^3; χ_M^{dia} is the molar diamagnetic contribution to the paramagnetic susceptibility calculated using Pascal's constants. The concentration (c) was recalculated for each temperature according to the changes in the solvent density (ρ): $c_T = m_c\rho/m_{sol}$, where mc is the weight of the complex, and msol is the weight of the solution.

DFT calculations. All calculations were performed with the ORCA 5.0.3 program package [42]. Geometry of the complex cations **[(bipy)$_4$Ni$_2$(L)]$^+$** and **[(phen)$_4$Ni$_2$(L)]$^+$** and the products of their oxidation, **[(bipy)$_4$Ni$_2$(L)]$^{2+}$** and **[(phen)$_4$Ni$_2$(L)]$^{2+}$**, was optimized using the B3LYP functional [33] with RIJCOSX approximation for Coulomb and HF integrals and def2-tzvp basis set. Solvation effects were accounted with CPCM continuum solvation model with dichloromethane as a solvent. The exchange constant for **[(bipy)$_4$Ni$_2$(L)]$^+$** was estimated by the broken symmetry approach as implemented in the ORCA 5.0.3 program package [43].

4. Conclusions

A modified Debus–Radziszewski procedure allowed us to produce a new ligand L with a N_2O_2 donor set that contains two phenolic and bridging imidazole moieties to provide an extended π-conjugated ligand framework. In the two binuclear complexes, **[(bipy)$_4$Ni$_2$(L)]Cl** and **[(phen)$_4$Ni$_2$(L)]Cl**, it mediates a weak antiferromagnetic interactions between the two Ni^{2+} ions with $J = -2.15$ cm^{-1}, as identified by variable-temperature dc-magnetometry. Attempts to introduce other metal ions, such as iron(III), copper(II), manganese(II) or cobalt(II), failed due to the disproportionation reaction of the hypothetical heteroleptic complexes.

One-electron electrochemical oxidation of both the ligand and the binuclear complexes produces unstable cation radicals with the lifetimes that can be potentially improved by the use of bulkier t-butyl groups in the *ortho*-positions of the ligand, often used to stabilize phenoxy radicals and prevent them from bis(μ-phenolate) dimerization [32]. As follows from quantum chemical calculations, the redox process is indeed centered on the ligand, with the spin density in the resulting cation-radical **[(bipy)$_4$Ni$_2$(L)]$^{2+}$** mostly localized on the phenolic and imidazole moieties of the ligand.

To produce mixed-valence complexes from the synthesized di(hydroxyphenyl)imidazolate **L** or similar ligands, other metal ions may be introduced, such as platinum or palladium, given the limited scope of substrates that we discovered. As an alternative pathway toward such complexes that may find use in molecular-sized devices [9], the bipyridine and phenanthroline co-ligands may be substituted for less sterically hindered ligands, such as ethylenediamine, to obtain binuclear metal complexes from a di(hydroxyphenyl)imidazolate ligand with t-butyl groups; otherwise, a steric bulk of these co-ligands does not allow such a complex to form.

Supplementary Materials: The following supporting information can be downloaded at: https://www.mdpi.com/article/10.3390/magnetochemistry8100132/s1, Figure S1: ^{1}H (top) and ^{13}C NMR (bottom) spectra of 1,2-bis(5-ethyl-2-hydroxyphenyl)ethane-1,2-dione.; Figure S2: ^{1}H spectra of 1,2-bis(5-ethyl-2-methoxyphenyl)ethane-1,2-dione.; Figure S3: ^{1}H (top) and ^{13}C NMR (bottom) spectra of 4,5-bis(5-ethyl-2-methoxyphenyl)-1H-imidazole.; Figure S4: ^{1}H (top) and ^{13}C NMR (bottom) spectra of 2,2′-(1H-imidazole-4,5-diyl)bis(4-ethylphenol.; Figure S5: ^{1}H NMR spectra of $[(bipy)_4Ni_2(L)](Cl)$.; Figure S6: ^{1}H NMR spectra of $[(phen)_4Ni_2(L)](Cl)$.; Figure S7: Variable-temperature magnetic susceptibility for a methanol solution of $[(phen)_4Ni_2(L)](Cl)$ from the Evans technique. Figure S8: α-LUMO orbital (0.03 isosurface level) for $[(bipy)_4Ni_2(L)]^{+}$ ($E^{LUMO} = -0.0887$ a.u.).; Figure S9: α-LUMO orbital (0.03 isosurface level) for $[(bipy)_4Ni_2(L)]^{2+}$ ($E^{LUMO} = -0.1007$ a.u.).; Figure S10: α-HOMO orbital (0.03 isosurface level) for $[(phen)_4Ni_2(L)]^{2+}$ (EHOMO = −0.1976 a.u.).; Figure S11: α-LUMO orbital (0.03 isosurface level) for $[(phen)_4Ni_2(L)]^{2+}$ ($E^{LUMO} = -0.1008$ a.u.).; Figure S12: Spin density (0.0065 isosurface level) for $[(phen)_4Ni_2(L)]^{2+}$.

Author Contributions: Conceptualization, V.V.N., I.A.N. and A.V.P.; methodology, V.V.N. and A.V.P.; validation, Y.V.N. and V.V.N.; formal analysis, Y.V.N.; investigation, I.A.N., K.M.K., D.Y.A., A.A.D. and K.A.S.; resources, V.V.N. and Y.V.N.; data curation, Y.V.N.; writing—original draft preparation, Y.V.N., I.A.N. and V.V.N.; writing—review and editing, Y.V.N., and V.V.N.; visualization, D.Y.A.; supervision, V.V.N. and A.V.P.; project administration, V.V.N. and A.V.P.; funding acquisition, V.V.N. All authors have read and agreed to the published version of the manuscript.

Funding: This work was supported by the Russian Foundation for Basic Research (grant No. 20-33-90295). Analytical and spectroscopic data were collected using the equipment of Center for molecular composition studies of INEOS RAS with the financial support of the Ministry of Science and Higher Education of the Russian Federation (Contract/agreement No. 075-00697-22-00).

Conflicts of Interest: The authors declare no conflict of interest.

References

1. Senthil Kumar, K.; Ruben, M. Emerging Trends in Spin Crossover (SCO) Based Functional Materials and Devices. *Coord. Chem. Rev.* **2017**, *346*, 176–205. [CrossRef]
2. Nikovskiy, I.; Polezhaev, A.; Novikov, V.; Aleshin, D.; Pavlov, A.; Saffiulina, E.; Aysin, R.; Dorovatovskii, P.; Nodaraki, L.; Tuna, F.; et al. Towards the Molecular Design of Spin-Crossover Complexes of 2,6-Bis(Pyrazol-3-Yl)Pyridines. *Chem. —Eur. J.* **2020**, *26*, 5629–5638. [CrossRef] [PubMed]
3. Tezgerevska, T.; Alley, K.G.; Boskovic, C. Valence Tautomerism in Metal Complexes: Stimulated and Reversible Intramolecular Electron Transfer between Metal Centers and Organic Ligands. *Coord. Chem. Rev.* **2014**, *268*, 23–40. [CrossRef]
4. Palii, A.; Aldoshin, S.; Tsukerblat, B. Mixed-Valence Clusters: Prospects for Single-Molecule Magnetoelectrics. *Coord. Chem. Rev.* **2021**, *426*, 213555. [CrossRef]
5. Poneti, G.; Mannini, M.; Sorace, L.; Sainctavit, P.; Arrio, M.-A.; Otero, E.; Criginski Cezar, J.; Dei, A. Soft-X-ray-Induced Redox Isomerism in a Cobalt Dioxolene Complex. *Angew. Chem. Int. Ed.* **2010**, *49*, 1954–1957. [CrossRef]
6. Gransbury, G.K.; Livesay, B.N.; Janetzki, J.T.; Hay, M.A.; Gable, R.W.; Shores, M.P.; Starikova, A.; Boskovic, C. Understanding the Origin of One- or Two-Step Valence Tautomeric Transitions in Bis(Dioxolene)-Bridged Dinuclear Cobalt Complexes. *J. Am. Chem. Soc.* **2020**, *142*, 10692–10704. [CrossRef]
7. Rajput, A.; Sharma, A.K.; Barman, S.K.; Saha, A.; Mukherjee, R. Valence Tautomerism and Delocalization in Transition Metal Complexes of O-Amidophenolates and Other Redox-Active Ligands. Some Recent Results. *Coord. Chem. Rev.* **2020**, *414*, 213240. [CrossRef]
8. Ohtsu, H.; Tanaka, K. Chemical Control of Valence Tautomerism of Nickel(II) Semiquinone and Nickel(III) Catecholate States. *Angew. Chem. Int. Ed.* **2004**, *43*, 6301–6303. [CrossRef]
9. Evangelio, E.; Ruiz-Molina, D. Valence Tautomerism: New Challenges for Electroactive Ligands. *Eur. J. Inorg. Chem.* **2005**, *2005*, 2957–2971. [CrossRef]
10. Thomas, F. Ligand-Centred Oxidative Chemistry in Sterically Hindered Salen Complexes: An Interesting Case with Nickel. *Dalton Trans.* **2016**, *45*, 10866–10877. [CrossRef]
11. Kurahashi, T. Drastic Redox Shift and Electronic Structural Changes of a Manganese(III)-Salen Oxidation Catalyst upon Reaction with Hydroxide and Cyanide Ion. *Inorg. Chem.* **2018**, *57*, 1066–1078. [CrossRef] [PubMed]
12. Glaser, T.; Heidemeier, M.; Fröhlich, R.; Hildebrandt, P.; Bothe, E.; Bill, E. Trinuclear Nickel Complexes with Triplesalen Ligands: Simultaneous Occurrence of Mixed Valence and Valence Tautomerism in the Oxidized Species. *Inorg. Chem.* **2005**, *44*, 5467–5482. [CrossRef] [PubMed]
13. Ito, N.; Phillips, S.E.V.; Stevens, C.; Ogel, Z.B.; McPherson, M.J.; Keen, J.N.; Yadav, K.D.S.; Knowles, P.F. Novel Thioether Bond Revealed by a 1.7 Å Crystal Structure of Galactose Oxidase. *Nature* **1991**, *350*, 87–90. [CrossRef]

14. Whittaker, M.M.; Kersten, P.J.; Nakamura, N.; Sanders-Loehr, J.; Schweizer, E.S.; Whittaker, J.W. Glyoxal Oxidase from Phanerochaete Chrysosporium Is a New Radical-Copper Oxidase (∗). *J. Biol. Chem.* **1996**, *271*, 681–687. [CrossRef] [PubMed]
15. Launay, J.-P. Electron Transfer in Molecular Binuclear Complexes and Relation with Electron Transport through Nanojunctions. *Coord. Chem. Rev.* **2013**, *257*, 1544–1554. [CrossRef]
16. Inagaki, A.; Yatsuda, S.; Edure, S.; Suzuki, A.; Takahashi, T.; Akita, M. Synthesis of Pd Complexes Combined with Photosensitizing of a Ruthenium(II) Polypyridyl Moiety through a Series of Substituted Bipyrimidine Bridges. Substituent Effect of the Bridging Ligand on the Photocatalytic Dimerization of α-Methylstyrene. *Inorg. Chem.* **2007**, *46*, 2432–2445. [CrossRef]
17. Pourrieux, G.; Fagalde, F.; Katz, N.E.; Parella, T.; Benet-Buchholz, J.; Llobet, A. Synthesis, Spectroscopic and Electrochemical Characterization and Molecular Structure of Polypyridyl Ruthenium Complexes Containing 4,4′-Azobis(Pyridine). *Polyhedron* **2008**, *27*, 2990–2996. [CrossRef]
18. Richardson, C.; Steel, P.J.; D'Alessandro, D.M.; Junk, P.C.; Keene, F.R. Mono- and Di-Nuclear Complexes of the Ligands 3,4-Di(2-Pyridyl)-1,2,5-Oxadiazole and 3,4-Di(2-Pyridyl)-1,2,5-Thiadiazole; New Bridges Allowing Unusually Strong Metal–Metal Interactions. *J. Chem. Soc. Dalton Trans.* **2002**, 2775–2785. [CrossRef]
19. Slater, J.W.; D'Alessandro, D.M.; Keene, F.R.; Steel, P.J. Metal–Metal Interactions in Dinuclear Ruthenium Complexes Containing Bridging 4,5-Di(2-Pyridyl)Imidazolates and Related Ligands. *Dalton Trans.* **2006**, 1954–1962. [CrossRef]
20. Rego, R.; Adriaensens, P.J.; Carleer, R.A.; Gelan, J.M. Fully Quantitative Carbon-13 NMR Characterization of Resol Phenol–Formaldehyde Prepolymer Resins. *Polymer* **2004**, *45*, 33–38. [CrossRef]
21. Ebel, K.; Koehler, H.; Gamer, A.O.; Jäckh, R. Imidazole and Derivatives. In *Ullmann's Encyclopedia of Industrial Chemistry*; John Wiley & Sons, Ltd: Hoboken, NJ, USA, 2000; ISBN 978-3-527-30673-2.
22. Yoke, J.T.; Weiss, J.F.; Tollin, G. Reactions of Triethylamine with Copper(I) and Copper(II) Halides. *Inorg. Chem.* **1963**, *2*, 1210–1216. [CrossRef]
23. Demaison, J.; Császár, A.G. Equilibrium CO Bond Lengths. *J. Mol. Struct.* **2012**, *1023*, 7–14. [CrossRef]
24. Alvarez, S. Distortion Pathways of Transition Metal Coordination Polyhedra Induced by Chelating Topology. *Chem. Rev.* **2015**, *115*, 13447–13483. [CrossRef] [PubMed]
25. Galadzhun, I.; Kulmaczewski, R.; Cespedes, O.; Yamada, M.; Yoshinari, N.; Konno, T.; Halcrow, M.A. 2,6-Bis(Pyrazol-1-Yl)Pyridine-4-Carboxylate Esters with Alkyl Chain Substituents and Their Iron(II) Complexes. *Inorg. Chem.* **2018**, *57*, 13761–13771. [CrossRef]
26. Boča, R. Zero-field splitting in metal complexes. *Chem. Rev.* **2004**, *248*, 757. [CrossRef]
27. Piguet, C. Paramagnetic Susceptibility by NMR: The "Solvent Correction" Removed for Large Paramagnetic Molecules. *J. Chem. Educ.* **1997**, *74*, 815. [CrossRef]
28. Koch, F.; Berkefeld, A.; Schubert, H.; Grauer, C. Redox and Acid–Base Properties of Binuclear 4-Terphenyldithiophenolate Complexes of Nickel. *Chem. —A Eur. J.* **2016**, *22*, 14640–14647. [CrossRef]
29. Ikezaki, A.; Nakamura, M.; Cheng, R.-J. Anomalous 13C NMR Chemical Shifts of High-Spin Saddle Shaped Manganese(III) Octaethyltetraphenylporphyrin Complexes. *Chem. Lett.* **2006**, *35*, 156–157. [CrossRef]
30. Arion, V.B.; Rapta, P.; Telser, J.; Shova, S.S.; Breza, M.; Lušpai, K.; Kožišek, J. Syntheses, Electronic Structures, and EPR/UV−Vis−NIR Spectroelectrochemistry of Nickel(II), Copper(II), and Zinc(II) Complexes with a Tetradentate Ligand Based on S-Methylisothiosemicarbazide. *Inorg. Chem.* **2011**, *50*, 2918–2931. [CrossRef]
31. Zheng, B.; Tang, F.; Luo, J.; Schultz, J.W.; Rath, N.P.; Mirica, L.M. Organometallic Nickel(III) Complexes Relevant to Cross-Coupling and Carbon–Heteroatom Bond Formation Reactions. *J. Am. Chem. Soc.* **2014**, *136*, 6499–6504. [CrossRef]
32. Jazdzewski, B.A.; Tolman, W.B. Understanding the Copper–Phenoxyl Radical Array in Galactose Oxidase: Contributions from Synthetic Modeling Studies. *Coord. Chem. Rev.* **2000**, *200–202*, 633–685. [CrossRef]
33. Bühl, M.; Reimann, C.; Pantazis, D.A.; Bredow, T.; Neese, F. Geometries of Third-Row Transition-Metal Complexes from Density-Functional Theory. *J. Chem. Theory Comput.* **2008**, *4*, 1449–1459. [CrossRef] [PubMed]
34. Radical Localization in a Series of Symmetric NiII Complexes with Oxidized Salen Ligands—Chiang—2012—Chemistry—A European Journal—Wiley Online Library. Available online: https://chemistry-europe.onlinelibrary.wiley.com/doi/abs/10.1002/chem.201201410 (accessed on 16 September 2022).
35. Yamaguchi, K.; Takahara, Y.; Fueno, T. Ab-Initio Molecular Orbital Studies of Structure and Reactivity of Transition Metal-OXO Compounds. In *Proceedings of the Applied Quantum Chemistry*; Smith, V.H., Schaefer, H.F., Morokuma, K., Eds.; Springer: Dordrecht, The Netherlands, 1986; pp. 155–184.
36. Noodleman, L.; Davidson, E.R. Ligand Spin Polarization and Antiferromagnetic Coupling in Transition Metal Dimers. *Chem. Phys.* **1986**, *109*, 131–143. [CrossRef]
37. Bencini, A.; Gatteschi, D. X.Alpha.-SW Calculations of the Electronic Structure and Magnetic Properties of Weakly Coupled Transition-Metal Clusters. The $[Cu_2Cl_6]^{2-}$ Dimers. *J. Am. Chem. Soc.* **1986**, *108*, 5763–5771. [CrossRef] [PubMed]
38. Fontaine, F.G. Cis-Bis(2,2-Bi pyridine) di chloro nickel(II) Methanol Solvate. *Acta Cryst. E* **2001**, *57*, m270–m271. [CrossRef]
39. Dolomanov, O.V.; Bourhis, L.J.; Gildea, R.J.; Howard, J.a.K.; Puschmann, H. OLEX2: A Complete Structure Solution, Refinement and Analysis Program. *J. Appl. Cryst.* **2009**, *42*, 339–341. [CrossRef]
40. Sheldrick, G.M. SHELXT—Integrated Space-Group and Crystal-Structure Determination. *Acta Cryst. A* **2015**, *71*, 3–8. [CrossRef]

41. Sheldrick, G.M. A Short History of SHELX. *Acta Cryst A* **2008**, *64*, 112–122. [CrossRef]
42. Neese, F. Orca 4.2.1. Wiley Interdiscip. *Rev. Comput. Mol. Sci.* **2012**, *2*, 73. [CrossRef]
43. Sinnecker, S.; Neese, F.; Noodleman, L.; Lubitz, W. Calculating the Electron Paramagnetic Resonance Parameters of Exchange Coupled Transition Metal Complexes Using Broken Symmetry Density Functional Theory: Application to a MnIII/MnIV Model Compound. *J. Am. Chem. Soc.* **2004**, *126*, 2613–2622. [CrossRef]